A-5 Biaxaial Tension, Distributed Dislocation Cores, and Fracture in Bubble Rafts

Frank A. McClintock[1]

and

William R. O'Day, Jr.[2]

Abstract

The bubble raft analogue of a crystal comes closer than a power function to describing the short-range repulsive forces at the small strains that govern fracture. The long-range attractive forces in both bubbles and metals mean that vacancies, stacking faults, and grain boundaries have little effect on the fracture strain, and even dislocations reduce the fracture strain by only a factor of two or three.

The core of a dislocation is described in terms of partial dislocations that are the vector sums of the non-linear displacements between the atoms over Burgers circuits containing as few as three atoms. Four types of distributed dislocation cores were observed, depending on the biaxial stress. The rather large sizes and distinct types of distributed dislocation cores make it difficult to predict fracture from linear elasticity and surface energy concepts.

In view of the low fracture strains for "hard" force laws, fracture will occur due to triaxial tension in front of a notch in such materials, before fully plastic flow can occur, if the ratio of flow stress to modulus of elasticity exceeds about 2%.

(1) Professor of Mechanical Engineering, Massachusetts Institute of Technology, Cambridge, Massachusetts, USA

(2) Mitron Research and Development Corporation, Waltham, Massachusetts, USA

Introduction

A bubble raft provides a two-dimensional model at a visible scale of edge dislocations in a crystal.

Previous studies (1, 2, 3) have been concerned with the configuration of dislocations or their motion in rafts under shear or uniaxial stress. These loadings have not produced fracture (except for one case involving dynamic loading (4)). In the present work, biaxial tension was applied to produce fracture. Biaxial tension corresponds to spalling in a real crystal, in which the reflection of stress waves produces high, nearly triaxial tension. It also simulates the state of stress in front of a sharp crack in a hard alloy. The crack cannot be modeled directly with a bubble raft because of the low stress required to move dislocations in a bubble raft in the absence of three-dimensional dislocation tangles, and the large rafts required for enough dislocations to simulate a plastic continuum.

Ideal Cohesive Strength and Strain

The classical calculation of the cohesion of a metallic crystal is that of Fuchs (5), shown in Fig. 1a. Although the value of the cohesive strength is largely determined by the slope of the attractive energy potential, the cohesive strain is determined by the high curvature of the repulsive potential as it falls to zero. Differentiation indicates a ratio of cohesive strength to bulk modulus of 0.09 at a strain of 0.045.

The attractive and repulsive energies are often approximated by a power law expression. To give zero stress at an equilibrium radius $r = r_o$, the energy per unit mass may be assumed to be of the form

$$U = A\left[\frac{1}{(r/r_o)^m} - \frac{m/n}{(r/r_o)^n}\right]. \qquad (1)$$

The radial stress is found by equating the change in energy of the mass $4\pi\rho_o r_o^3/3$ to the work done, and then rearranging the equation:

$$\sigma_r = \frac{\rho_o A m}{3}\left[\frac{-1}{(r/r_o)^{m+3}} + \frac{1}{(r/r_o)^{n+3}}\right]. \qquad (2)$$

The radius at which the stress is a maximum turns out to be

$$\frac{r_c}{r_o} = [(m+3)/(n+3)]^{1/(m-n)}. \qquad (3)$$

The ratio of ideal cohesive strength to bulk modulus is σ_c/B. This would be the volumetric strain at σ_c if the behavior were linear. The corresponding normal component of strain, $\sigma_c/3B$, is easier to compare with the cohesive

strain (at the cohesive strength), $(r_c - r_o)/r_o$:

$$\frac{\sigma_c}{3B} = \left(\frac{1}{m-n}\right)\left[\left(\frac{n+3}{m+3}\right)^{\frac{n+3}{m-n}} - \left(\frac{n+3}{m+3}\right)^{\frac{m+3}{m-n}}\right]. \qquad (4)$$

The ratio of bulk modulus to binding energy per unit volume, $B/\rho_o|U_o|$, is

$$B/\rho_o|U_o| = mn/9. \qquad (5)$$

The attractive force is relatively long range. For an ionic crystal the exponent n is 1, and Fuchs' calculations indicate an even flatter relation for copper. For the repulsive energy, the results for a number of values of the exponent m are presented in Table 1, along with the results of Fuchs' calculations. A very large value of m is required to simulate the high curvature in the repulsive force law near the cohesive strength, but then the magnitude of the energy is in error. No value of m seems to give a good fit for copper. For the alkali metals Seitz (6) suggests m = 3, except for lithium for which m = 2 is a better value.

For bubbles, the force law has been accurately calculated and experimentally verified by Lomer (7, 8), and is summarized in Table 2. Here again there is a high curvature of the repulsive potential as the cohesive strength is approached, and the bubbles lose contact with each other. For a two-dimensional array, Eqs. 3 and 4 take on the form

$$\sigma_r = C\left[\frac{-1}{(r/r_o)^{m+2}} + \frac{1}{(r/r_o)^{n+2}}\right], \qquad (7)$$

$$r_c/r_o = [(m+2)/(n+2)]^{1/(m-n)}, \qquad (8)$$

with corresponding changes in the other equations, which are not of interest here. The results for various values of the repulsive exponent m, in Table 2 indicate that again it is not possible to choose a value of m that gives a good fit. It thus appears that the bubble model is a better representation of the cohesive behavior of copper than any simple power law. Similar difficulties would be encountered with a Born-Mayer type of exponential law for the repulsive force. As suggested by Lomer and shown in Fig. 1b, taking a dimensionless bubble size of about $\alpha = 0.4$ (1.2 mm bubble diameter) gives the best fit in terms of the ratio of slope to ordinate of the potential at the equilibrium spacing. For similar curvatures, this would give identical cohesive strains.

Representation of Distributed Dislocation Cores by Partial Burgers Vectors

Viewed in cross-section, the core of a dislocation is not a point, but

is spread out, as shown by the examples of Fig. 2. The spreading out increases with transverse tension, as we shall see here, and with thermal motion, as noted by Fukushima and Ookawa (3). The types of dislocations can be divided into two broad categories, depending on whether or not, at the center of the dislocation, atoms or interstices were across the slip plane from each other. The types could be further classified according to the shape of their regions of maximum misfit: straight, V-shaped, or triangular.

As a concise shorthand for these various types, the convention was adopted that the extra half planes (heavy lines) of the conventional representation would be drawn to meet the slip line (light line) at the same point for atom-centered types, but would meet the slip line at separate points for interstice-centered types. On the tensile side of the slip plane the regions of lowest density are shown by dashed lines, giving the diagrams shown in Fig. 2.

These dislocations can be described more quantitatively by describing how much of the dislocation strength lies within any polygon formed by as few as three atoms. This strength will be termed the partial Burgers vector. In the past, this term has been applied to partial dislocations bounding a stacking fault. These have discrete crystallographic orientation and magnitude. The much smaller partial Burgers vectors considered here might be called "hyper-partial" dislocations, but such emphasis is probably not needed. Partial Burgers vectors can be found from the relative displacements (from the dislocation-free state) around a small triangular circuit connecting three atoms in the lattice, by adapting Kröner's (9) ideas for continuous arrays of dislocations. See also Kondo and Yuki (10). The line integral of the relative displacement around a circuit is zero, but it can be thought of as consisting of the sum of linear and non-linear vector parts (termed "elastic" and "plastic" by Kroner):

$$d\bar{w} = 0 = d\bar{w}^{\ell} + d\bar{w}^{n}. \qquad (9)$$

The separation of the displacement into linear and non-linear parts can be made if a force law can be defined for pairs of atoms. The parts of the relative displacements are those which would be found for the assumed forces if the force law were linear, as shown in Fig. 3. The fraction of a dislocation contained within a triangular circuit is given by either the linear or non-linear integral of Eq. 1, with the sign taken to be that of the integral of the linear displacements.

Note that for a circuit around a large number of atoms containing a unit or perfect dislocation, the line integral is taken through material which is very nearly linear, except for the point of the circuit through which the dislocation entered. Integrating the linear relative displacements around a circuit that would close in a reference crystal gives the usual Burgers vector. On the other hand, the integral of the non-linear displacements is zero except for the element through which the dislocation entered. If the force law is chosen so the force vanishes for a unit displacement, then for this element the non-linear displacement is the negative of the Burgers vector. Thus the line integrals of Eq. 9 reduce to the conventional definition for Burgers vectors of unit size.

It is evident from Fig. 3 that the magnitude of a partial Burgers vector depends on the shape of the interatomic force law. Since unit displacements in a lattice return the force to zero, the force should depend in a periodic way on the relative displacements. Furthermore, the force law should be chosen so as to give the same configuration whether the dislocation has come in from one direction or the other, even though the displacements are different. This is accomplished by making it anti-symmetrical, as well as periodic. Finally, since the very concept of a pair-wise interatomic force law is already an approximation, it is not unreasonable to assume for simplicity that the force law consists of straight line segments, as shown in Fig. 4. The linear and non-linear parts of the relative displacement vector are taken to be co-linear with the total relative displacement vector.

To gain insight into this representation of distributed dislocation cores, consider the modes of deformation of a triangle shown in Fig. 5. Because the definition is based on relative displacements, there is no effect of rigid body translation. Rigid body rotation and pure dilatation of equilaterial triangles or squares produce equal relative displacement vectors that form regular polygons and sum to zero. The non-linear parts also form regular polygons that sum to zero. Combined translation and rotation, shown in Fig. 5a, is no different from pure rotation. In Fig. 5b, the relative motion of just one atom produces no net Burgers vector because the two non-zero relative displacements cancel. The equivalent isoceles deformation of Fig. 5c, which is similar but with a superimposed rotation, does have a Burgers vector (Fig. 5c). This dependence on rotation is neither surprising nor unrealistic in view of the non-central nature of the force field. It means that the coordinates used for each triangle must have the same orientation, although they may have different origins.

Ideally, the choice of the triangular net should be immaterial. Actually, there is an effect, as illustrated in Fig. 6, for an idealized straight edge dislocation. In Fig. 6a, the relative displacements were those which would arise from a dislocation sliding in from the right. In Fig. 6b, the relative displacements are those resulting from condensation of two half-planes below the slip plane. Care must be taken that the topology of the reference net is preserved, so that a collapsed set of triangles, one containing a small partial Burgers vector, appears in Fig. 6b at the site of the missing half plane. Alternatively, the partial Burgers vectors may be drawn on the original reference lattice as shown in Fig. 6c. This representation has the advantage of focusing attention on the Burgers vectors rather than on the deformation of the grid, but some of the symmetry and a feeling for the deformation of the lattice are lost.

The one free parameter in a force law of the idealized type shown in Fig. 4 is the relative displacement at the cohesive strength. For such a large value as $w_c/b = 0.25$, used in Fig. 6, the relative displacements of nearly all triangles are completely within the linear range and hence most triangles have no net Burgers vector. The dislocation then appears concentrated near its core. With a lower value of the critical relative displacement, $w_c/b = 0.10$, the partial Burgers vectors are more spread out, as shown in Fig. 7.

From Tables 1 and 2, a more realistic critical relative displacement is $w_c/b = 0.05$. In order to reduce the computation time, a computer program

was developed which accepted as input both the coordinates of the bubbles and a tabulation of which bubbles belonged to each triangle. The computer, through a plotter, produced a diagram of the deformed grid and the partial Burgers vectors (complete with arrow-heads). A memorandum describing the program and a program listing in the Fortran language are available on request. The resulting arrays of partial Burgers vectors are shown in Fig. 8 for each of the types of dislocations of Fig. 2. Areas where adjacent vectors are the only non-linear ones in a triangle give pairs of equal and opposite arrows. These arrows are much reduced if the critical displacement w_c/b is taken to be 0.10 instead of 0.05, as can be seen from a comparison of Figs. 8a-1 and 8a-2.

Experimental Procedure

Biaxial tension was produced by the equal outward motion of the three vertices of an equilateral triangle of rubber strips. This triangular boundary, to which the bubbles adhered well, was partially submerged in a bubble solution of the type used by Bragg and Nye (1). The necessary measurements were taken from motion pictures.

Even the "perfect" rafts occasionally had two or three bubbles perhaps 15% undersized. If these were not close together fracture often occurred elsewhere, so the rafts did not appear to be weakened.

Prestrains of +1 to -4% were present in the rafts, depending on the original dimensions of the triangular boundary, the size of bubbles used, and the amount of breaking or adding of bubbles necessary to get the desired raft. The equilibrium spacing was therefore determined from a freely floating bubble patch after fracture.

To evaluate the error in strain measurement, about thirty readings were made of ten-bubble rows in one free-floating patch. The scatter amounted to about 1% strain.

To estimate the magnitude of viscous effects, a run which contained the transition from a V-type to an atom-centered triangular dislocation was analyzed. Fig. 9 shows the variation of strains, both internal and external, with time. The transition took place in something less than two seconds, negligible compared to the 50 to 100 seconds required for a typical run.

Fracture strains

a. Perfect lattice. The data for perfect rafts are shown in Fig. 10a. The vertical bar indicates 95% confidence limits for the mean strength, obtained by extrapolating the fracture strains for all diameters to a common value of 1.2 mm along the approximate least squares line which is shown. Assuming a normally distributed population, the confidence limits were obtained from the range of the sample, using convenient plots (11).

Because the attractive forces are so long range, the strain required to reach the cohesive strength is the equilibrium compression Δ_o given by

Lomer ((7), Fig. 2 and (8), Fig. 3)[1]. The data are about 30% below the theory, which is not surprising in view of the uncertainties of measurement and the possible variations in bubble size.

b. Single dislocations. Data from rafts containing single dislocations are shown in Figs. 10b, c, and d, classified according to the type of dislocation existing at fracture. In many runs an initially atom-centered, straight dislocation transformed to the interstice-centered V-type, and sometimes later to one of the triangular types. The Burgers vectors are unaffected by these transitions. Very seldom did fracture occur from a V-type dislocation before the transition to the atom-centered triangular type. Because of this, and because the fracture strains of the two types were not significantly different, both were included in Fig. 10c. The transformations seemed to be reversible, judging from a few experiments in which the straining was changed from tension to compression and back again.

In spite of the experimental uncertainty, it appears that the V-type and triangular dislocations reduce the fracture strain by about a factor of two from the experimental data for the perfect lattice. With perfectly uniform bubbles, one would expect the reduction in strength to be somewhat greater, perhaps a factor of three, since any reduction in fracture strain due to uneven bubble size is more likely to appear in the perfect raft than in one with a dislocation, where the fracture must occur at the dislocation.

As regards mode of fracture, the perfect rafts usually cleaved in what would be a $\langle 112 \rangle$ direction in a face-centered cubic crystal. In the one exception, two $1/2\langle 111 \rangle$ dislocations of opposite sign nucleated spontaneously and separated to create a stacking fault which then cleaved. The straight dislocations cleaved parallel to the Burgers vector, although occasionally odd bubbles stuck to the wrong side of the crack. The vee and triangular types tended to cleave on one of the $\langle 111 \rangle$ directions at 60° to the Burgers vector, shown as dotted lines in schematic diagrams of Fig. 2, but frequently changed from one of the two directions to the other.

One possible analysis for the sensitivity of dislocations to tension arose from the observation that the width of straight edge dislocations increases under tension. Since the growth to infinite width would contribute to fracture, it was considered as a limiting case. Following the analysis of Lomer (8) for the force acting across a section in the raft, the potential V can be given in terms of a function of the bubble size, $\emptyset$, the characteristic range of action of the meniscus, a_o, defined in Table 1, the dimensionless bubble radius α, and the spacing $\overline{}$ between the planes, d, by

$$V = \frac{1.705\ \emptyset}{\alpha} \sum_{n=1}^{\infty} n e^{-nd/a_o} \quad .$$

[1] Δ of (8), Table 3 is not quite consistent with this, but agreement is found from $\Delta_o = \delta_o (1 + 2\gamma)$, with δ_o from (8), Table 4 and γ from (8), Table 3.

As the dislocation grows to infinite width, the stacking across the plane of the dislocation changes from the hexagonal close-packed to the simple cubic type. The effect is to increase each distance between a pair of planes across a crack by the amount $2R(1-\sqrt{3}/2)$. In terms of $R/a_o = \alpha$, the potential is then changed by the factor $e^{-(2-\sqrt{3})\alpha}$. In order for this transformation to occur it is necessary that the work done by the applied stresses acting through this displacement be equal to the change in potential energy. In Table 3 the required forces are compared with the theoretical strength of the raft for bubbles of various sizes. Because the attractive force is so long range and the force falls off so slowly with increasing spacing, the stress must be very nearly equal to the theoretical strength before the dislocation widens. Therefore, the widening effect per se was not expected to, and in fact did not, play a large role in the initiation of fracture from dislocations.

A second analysis which might shed light on fracture from dislocations is that due to Stroh (12). (See also Bullough (13)).

This analysis requires the variables of Table 4, which were evaluated from Lomer's study of interatomic forces. The resulting equation, plotted in Fig. 11, is

$$a = \frac{4\mu}{\pi T^2(1-\nu)}\left[\gamma - \frac{n\lambda T}{4} \pm \gamma\left(1 - \frac{n\lambda T}{2\gamma}\right)^{1/2}\right] .$$

This analysis indicates a crack length roughly that of the size of the highly strained region in the triangular type of dislocation. On the other hand, the analysis indicates a higher fracture strain than observed, and fails to indicate the strong effect of bubble diameter. Evidently, the linear theory in this form is inadequate to explain the phenomenon in view of the highly non-linear and long-range forces.

c. Vacancies or dislocation pairs. Geometrically, a row of several vacancies can be thought of as a pair of edge dislocations of opposite signs on parallel planes. The vacancies might form a crack and thus be more serious than separate dislocations. Actually, the vacancies did not form a crack which then split open, but rather formed multiple vacancy arrays of the type previously reported (2,3). Arrays with four or fewer vacancies had little effect on the fracture strain, as indicated in Fig. 12. Direct evidence for the high strain was obtained from the fact that in one case a dislocation spread as a stacking fault all the way from a vacancy array to a boundary and even reflected from the boundary, as shown in Fig. 13. Judging from the preceding analysis for a stacking fault, the strain in this case must have been within a very few per cent of the theoretical strain, although the measurements had indicated a somewhat lower value. Even for arrays of nine vacancies, dislocation pairs did not form. Although the strength decreased, it did not appear to drop below that of individual or isolated dislocations.

An estimate of the applied strains required for dislocations to produce cracks which then fracture can be made by assuming that the critical part of the process is the growth of a crack from either dislocation about a third of the way towards the other, during which time interaction effects may be neglected. The resulting curve, shown in Fig. 12, again indicates the insufficiency of the linear theory.

d. Grain boundaries. For these experiments the straining frame was enlarged from 7 cm to 10 cm on a side to accommodate rafts containing a single grain in the center. Almost all the grains had a 30° orientation relative to each other, as in Fig. 14. The summary of results in Table 5 indicates that fractures tended to occur where the grain boundary was parallel to one of the close packed rows rather than where it made an angle of 15° with the close packed rows in each grain. Again the long-range action of the attractive forces played an important role, here by making the atoms adhere closely either to one grain or the other, and by maintaining the attractive force between the grains even over a relatively large separation. As a result the grain boundary strengths were nearly identical with those of the perfect rafts, as shown in Fig. 15.

Ultimate Notch Toughness of Crystals

Judging from these results, even in ductile materials a strain of the order of two per cent under triaxial tension will open up dislocations and thus cause numerous fracture nuclei. These nuclei will in turn give macroscopic fracture by the growth and coalescence of holes. If this conclusion is correct and applicable to steel, the highest strength steel that could be made insensitive to notches can be estimated by taking the mean normal stress to be that found in the fully plastic, plane strain, externally notched case, $(1+\pi)Y/\sqrt{3}$. The required yield strength Y for a mean normal strain of 2% is then found from

$$.02 = \frac{Y(1+\pi)}{\sqrt{3}}\,\frac{1-2\nu}{E}$$

For steel with $\nu = 0.3$ and $E = 30 \times 10^6$ psi, this leads to $Y = 600{,}000$ psi. While higher strength steels might be made, they would not be notch-tough in the sense of being able to carry the fully plastic stress distribution of approximately three times the yield strength.

Experiments on scabbing by O'Brien and Davis (14) indicated fracture at 200,000 psi of nearly hydrostatic tension in all kinds of aluminum ranging from zone-refined single crystals to high strength alloys. The corresponding strain is

$$\varepsilon = \frac{\sigma(1-2\nu)}{E} = .0067,$$

rather below the 2% strain found here for copper. It remains to be determined whether this difference is due to approximations in the interatomic force laws or to fracture by more complex mechanisms.

Conclusions

1. The fracture strain in a perfect lattice is largely determined by the nature of the repulsive forces, and ranges from perhaps 20% for alkali metals to 4% for noble metals. The bubble raft analogy to a crystal structure comes closer than a power function to describing the short range repulsive forces in the small tensile strains that govern fracture.

2. The long range attractive forces in both bubbles and metals mean that vacancies, stacking faults, and grain boundaries produce little weakening, and even dislocations reduce the fracture strain by only a factor of two or three.

3. Especially under triaxial tension, dislocations involve non-linear displacements over many atoms per cross-sectional plane. Four types of such diffuse dislocations are described. The large sizes and distinct types of diffuse dislocations prevent prediction of fracture from simple linear elasticity and surface energy concepts.

4. The distribution of fractional dislocations throughout the core of a dislocation can be described in terms of the linear or non-linear parts of the relative displacements between atoms in a Burgers circuit containing as few as three atoms.

5. The low fracture strains mean that for hard metals, full plasticity in the presence of a notch cannot be maintained if the ratio of yield strength or flow stress to modulus of elasticity exceeds about 2%.

Acknowledgment

The authors wish to thank Stuart E. Madnick, for his programming of the computer plotting procedure, and Peter D. McMorran for his painstaking measurement and recording of hundreds of needed coordinates. Computations were carried out through the courtesy of the Computation Center at M.I.T. Financial support of the National Science Foundation through grants G-14995 and GP-2838 is gratefully acknowledged.

References

1. L. Bragg and J. F. Nye, Proc. Roy. Soc. A, 190, 474 (1947).

2. L. Bragg and W. M. Lomer, Proc. Roy. Soc. A, 196, 171 (1949).

3. E. Fukushima and A. Ookawa, J. Phys. Soc. Japan, 10, 970 (1955). (See also 12, 139 (1957)).

4. J. J. Gilman, Trans. AIME, 212, 783 (1958).

5. K. Fuchs, Proc. Roy. Soc. A, 151, 585 (1935). See also 157, 444 (1936)).

6. F. Seitz, The Modern Theory of Solids, McGraw-Hill, New York, 381 (1940).

7. W. M. Lomer, Proc. Roy. Soc. A, 196, 182 (1949).

8. W. M. Lomer, Proc. Camb. Phil. Soc., 45, 660 (1949).

9. E. Kroner, Ergebnisse der Angewandten Mathematik, 5, Springer, Berlin, 18 (1958).

10. K. Kondo and M. Yuki, Memoirs of the Unifying Study of the Basic Problems in Engineering Science and Physical Sciences by Means of Geometry, 2, Gakujutsu Bunken Fukyu-Kai, Tokyo, 202 (1958).

11. F. A. McClintock, Metal Fatigue, G. Sines and J. L. Waisman, Eds. McGraw-Hill, 136 (1959). (For tables see R. A. Risher and F. Yates, Statistical Tables for Biological, Agricultural and Medical Research, Fourth Ed. Oliver and Boyd, Ltd., Edinburgh and London, Table 3, (1953)).

12. A. N. Stroh, Advances in Physics, 6, 418 (1957).

13. R. Bullough, Phil. Mag., 9, 917 (1964).

14. J. L. O'Brien and R. S. Davis, Response of Metals to High Velocity Deformation, AIME Metallurgical Society Conf. 9, Interscience, New York, 371 (1961).

Table 1

Ideal Strengths and Strains for 3-Dimensional Lattices

Approximation	Parameter m	Parameter n	Strain $(r_c-r_o)/r_o$	Strength $\sigma_c/3B$
Power law (3 dimensional)	3	1	0.225	0.074
	5	1	0.189	0.0625
	9	1	0.147	0.0482
	13	1	0.122	0.039
Copper, from Fuchs (5)			0.045	0.03

Table 2

Cohesive Strains for Two-Dimensional Lattices

Approximation	Parameter m	Parameter n	Cohesive Strain $(r_c-r_o)/r_o$
Power law	3	1	0.290
	5	1	0.236
	9	1	0.176
	13	1	0.144

Bubble raft	$\alpha_o = r_o/a_o$	d_o for a_o = 1.5 mm	
	0.2	.6	0.0185
	0.4	1.2	0.044
	0.6	1.8	0.076
	0.8	2.4	0.106
	1.0	3.0	0.115

$a_o = \sqrt{T/\rho g}$, where T is surface tension and ρg is weight density. For typical solution used with bubble rafts, a_o = 1.5 mm.

Table 3

Stress Required for Infinite Stacking Fault

Dimensionless bubble size, α	0.2	0.4	0.6	0.8	1.0
Binding energy=2(surface tension), dyne	.102	.38	.748	1.08	1.24
Faulting stress, dyne/cm	.670	2.425	4.67	6.00	7.36
Theo. strength, dyne/cm	.680	2.566	5.05	7.30	8.38
Ratio	.971	.949	.926	.905	.879

Table 4

Parameters for Elastic Calculation of Crack Length

Variable	Symbol	Units	Dimensionless bubble radius, α = 0.2	α = 0.4
Young's modulus	E	dyne/cm	27.7	37.7
Poisson's ratio	ν	---	0.438	0.50
shear modulus	μ	dyne/cm	9.56	12.6
number of dislocations	n=1			
Burgers vector	λ	cm	0.06	0.12
surface energy	γ	dyne	0.051	0.19
applied stress	T	dyne/cm		
crack length	a	cm		

Table 5

Grain Boundary Angles at Point of Fracture

Angles defined in Fig. 14

Bubble size mm	Fracture strain	Angles, degrees θ_i	θ_o	$\theta_i + \theta_o$
.93	.025	25	3	28
.87	.032	32	2	34
.86	.036	15	25	40
1.08	.051	32	3	35
1.06	.014	3	23	26
1.50	.036	3	19	22
1.50	.028	20	5	25

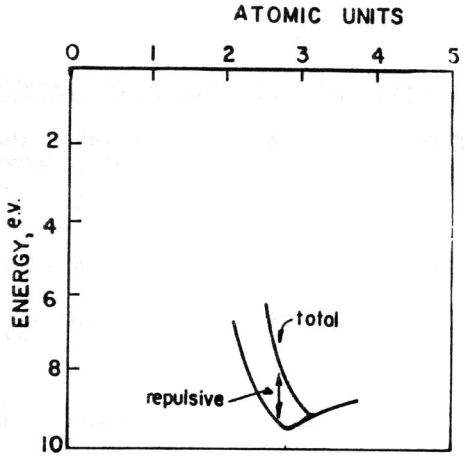

Fig. Ia. BINDING ENERGY FOR COPPER

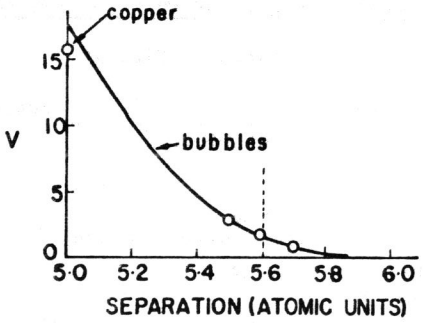

Fig.Ib. THE REPULSIVE POTENTIALS FOR COPPER AND 1.8mm BUBBLES AFTER LOMER (8).

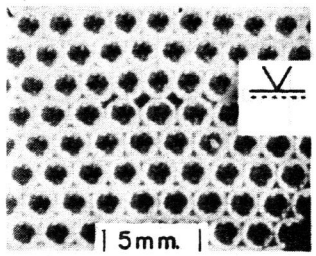

a. STRAIGHT ATOM-CENTERED

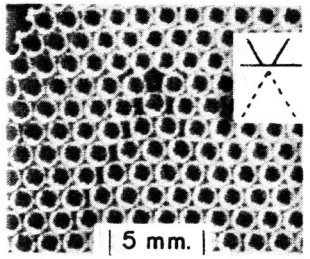

b. INTERSTICE-CENTERED V-TYPE

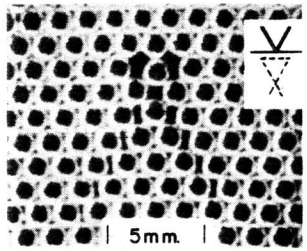

c. ATOM-CENTERED TRIANGULAR

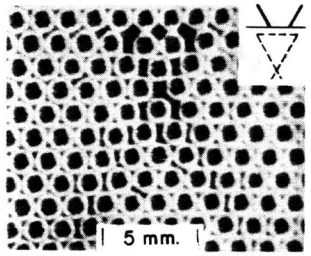

d. INTERSTICE-CENTERED TRIANGULAR

Fig. 2. TYPES OF DISLOCATIONS

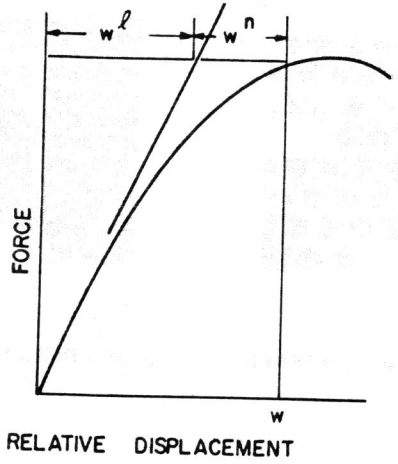

Fig 3 LINEAR AND NON-LINEAR PARTS OF THE RELATIVE DISPLACEMENT.

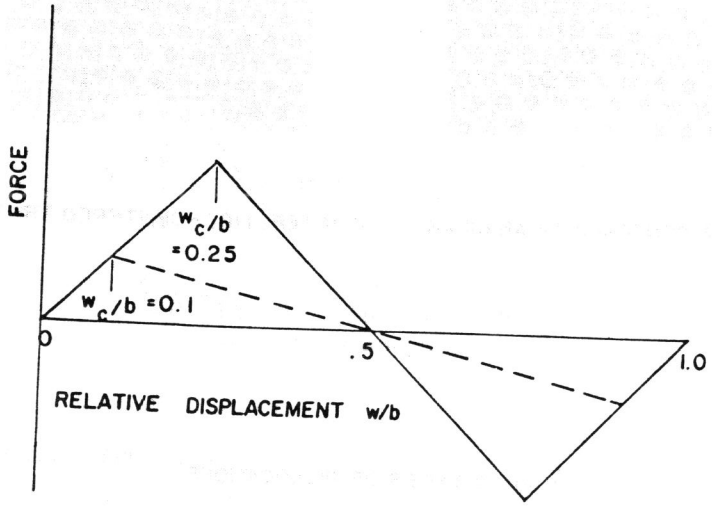

Fig 4 IDEALIZED RELATION BETWEEN FORCE AND RELATIVE DISPLACEMENT.

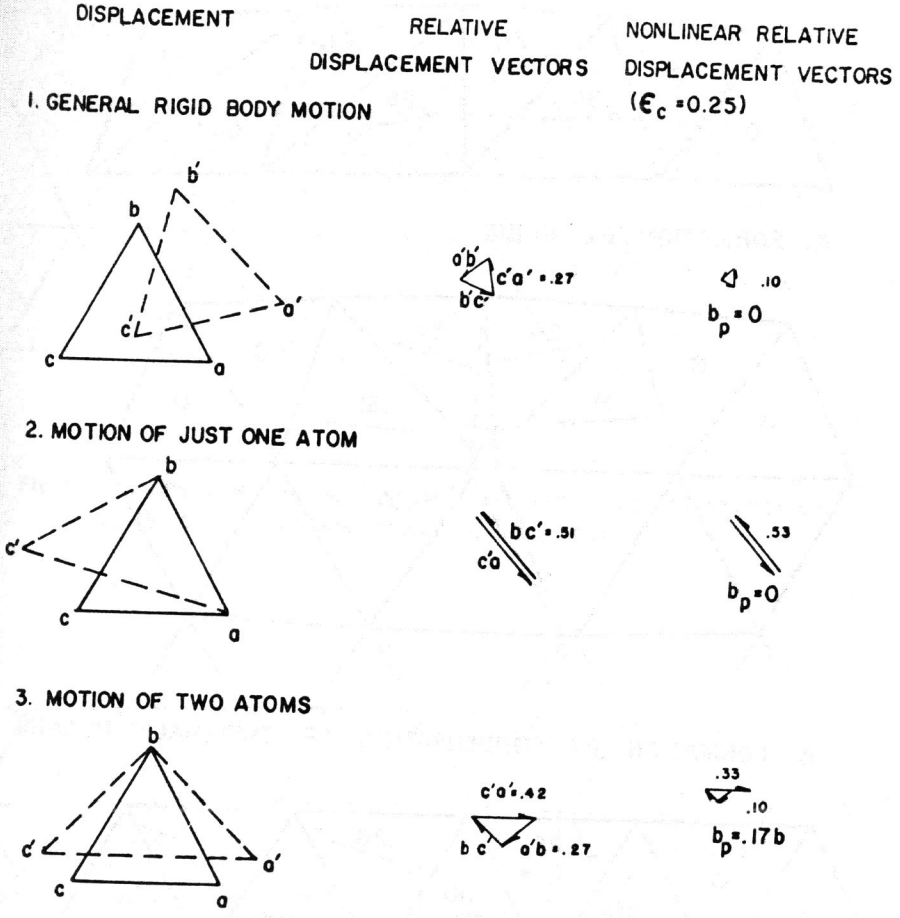

Fig.5 PARTIAL BURGERS VECTORS FOR TYPICAL DISPLACEMENTS (PER UNIT LATTICE SPACING)

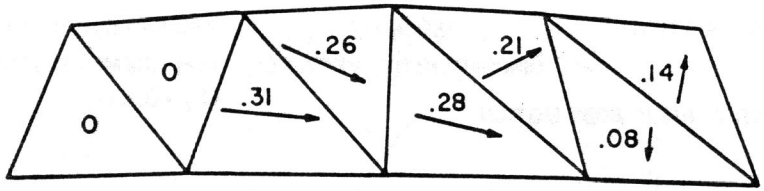

A. FORMATION BY GLIDE

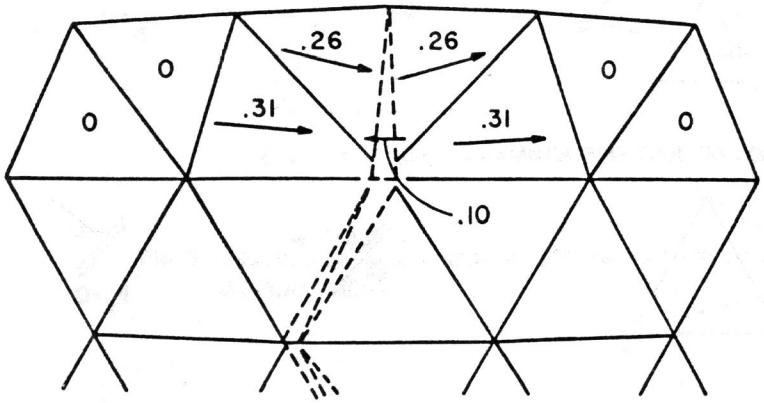

B. FORMATION BY CONDENSATION OF TWO HALF PLANES

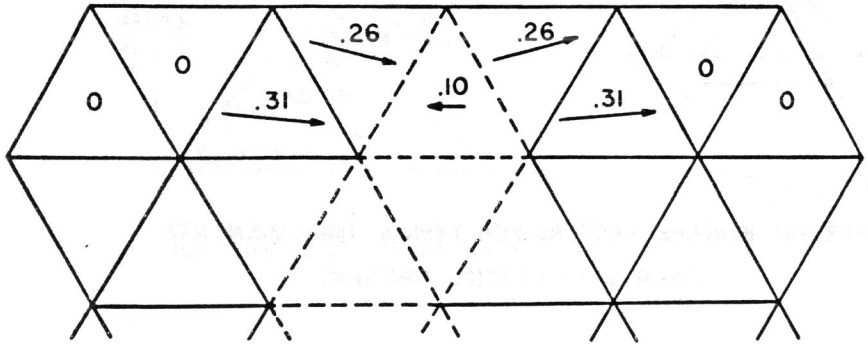

C. PARTIAL BURGERS VECTORS ON REFERENCE LATTICE

Fig.6 CHOICE OF REFERENCE LATTICE FOR IDEALIZED DISLOCATION $w_c/b = 0.25$. VECTORS DRAWN DOUBLE SIZE

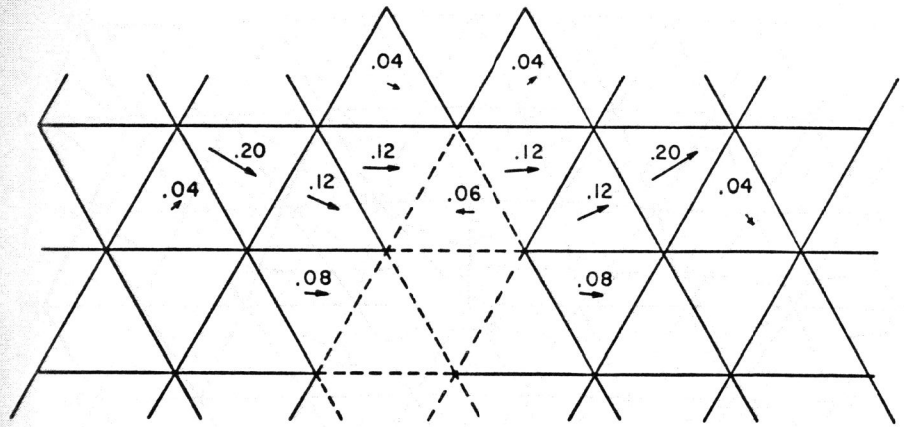

Fig.7 VECTORS FOR "HARDER" FORCE LAW AND IDEALIZED DISLOCATION $w_c/b = 0.10$. VECTORS DRAWN DOUBLE SIZE

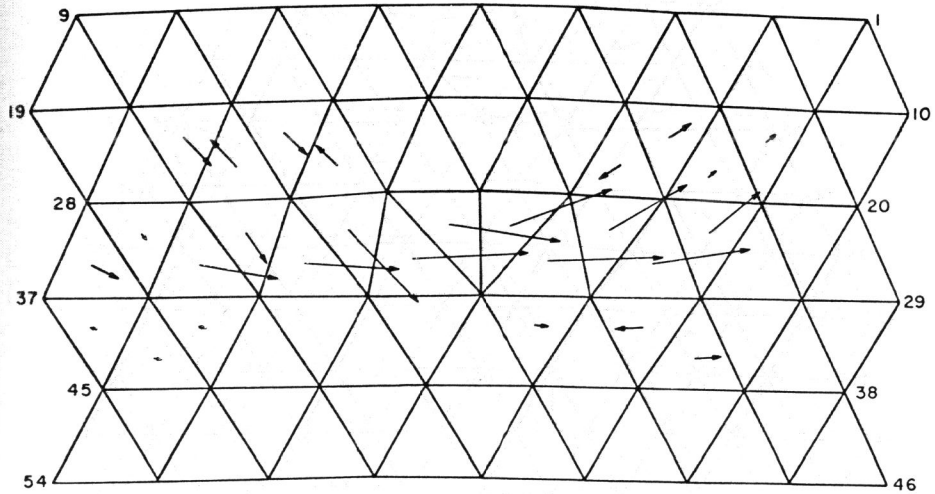

Fig. 8a-1 ATOM-CENTERED EDGE DISLOCATION $w_c/b = 0.10$. VECTORS DRAWN 10x

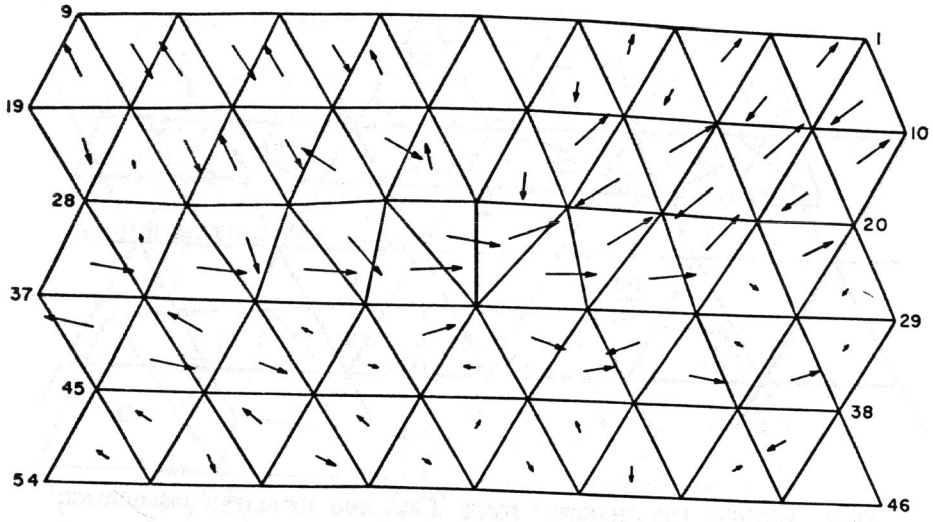

Fig. 8a-2 ATOM-CENTERED EDGE DISLOCATION
$w_c/b = 0.05$. VECTORS DRAWN 10x

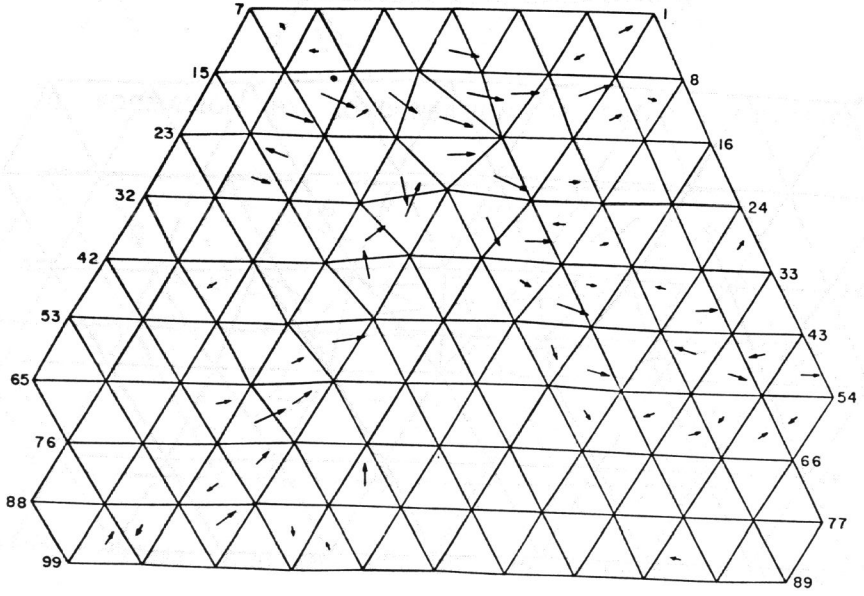

Fig. 8b INTERSTICE-CENTERED V-TYPE DISLOCATION
$w_c/b = 0.05$. VECTORS DRAWN 10x

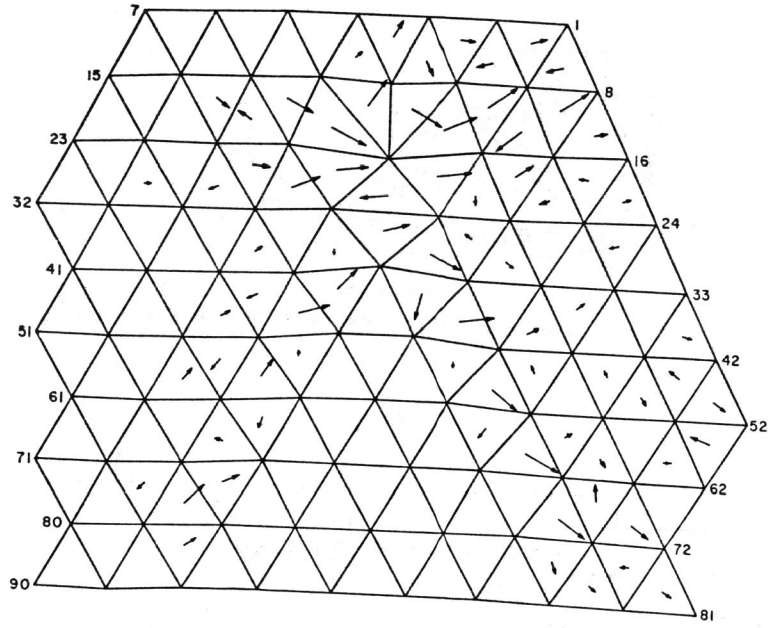

Fig. 8c ATOM-CENTERED TRIANGULAR DISLOCATION
$w_c/b = 0.05$. VECTOR DRAWN 10x

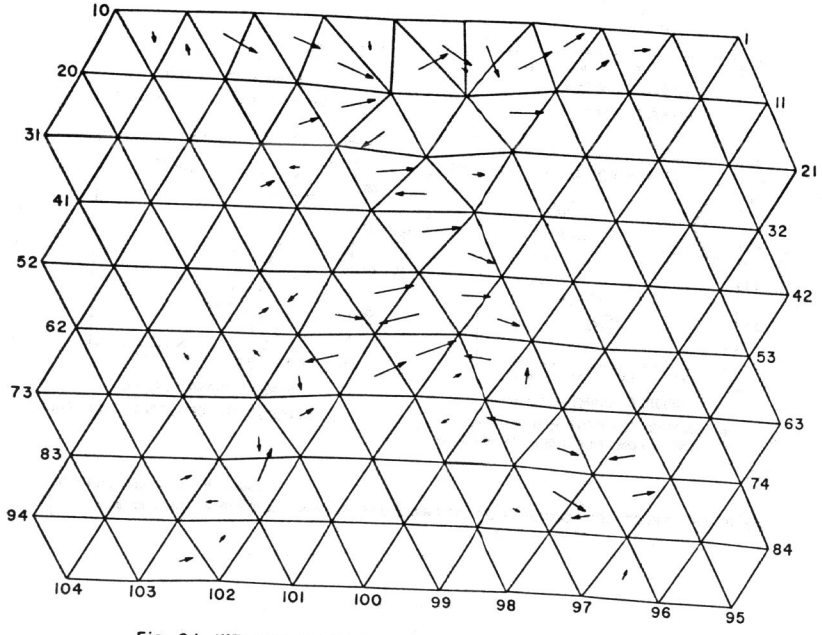

Fig. 8d INTERSTICE-CENTERED TRIANGULAR DISLOCATION
$W_c/b = 0.05$. VECTORS DRAWN 10_x

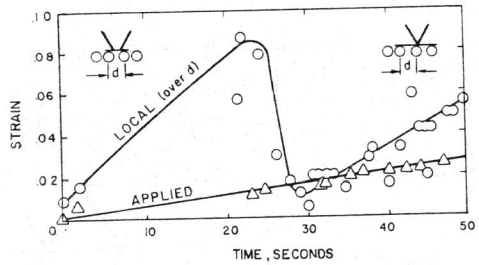

Fig. 9 ABRUPTNESS OF A DISLOCATION TRANSFORMATION

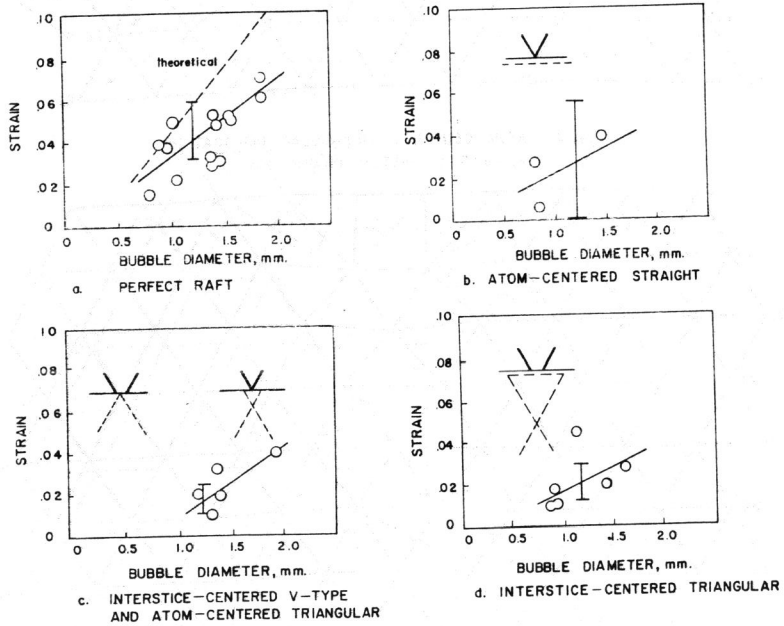

Fig. 10 THE EFFECT OF A DISLOCATION ON FRACTURE STRAIN (I shows 95 % confidence limits assuming indicated slope)

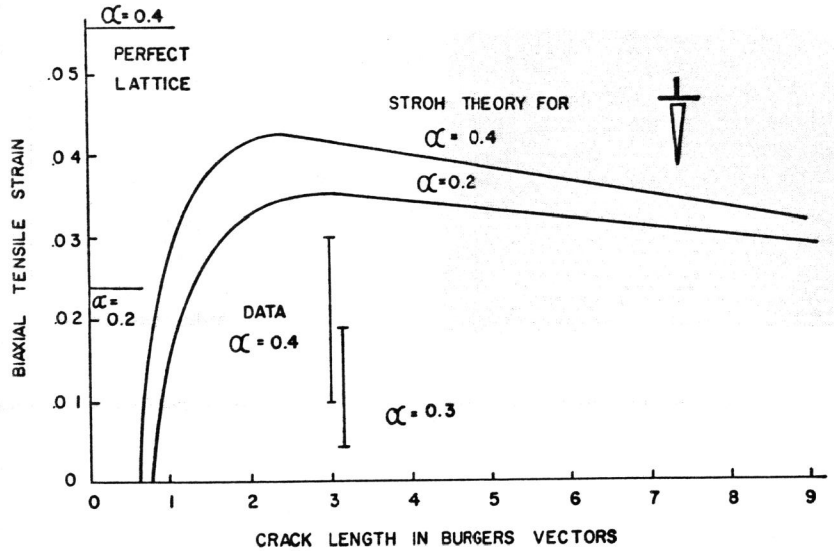

Fig. 11 GROWTH OF A CRACK FROM A DISLOCATION.
PEAK OF CURVE GIVES STRENGTH WITH ONE DISLOCATION.

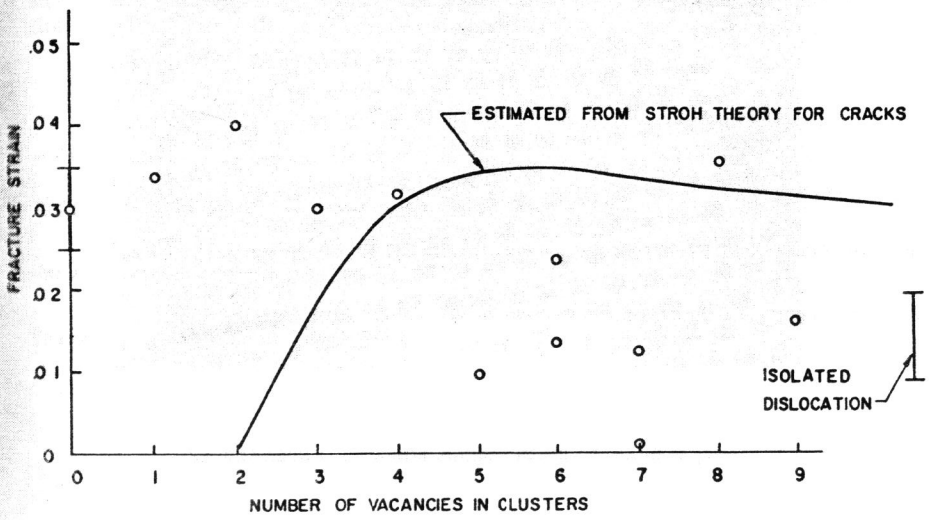

Fig. 12 FRACTURE STRAIN VS. NUMBER OF VACANCIES
BUBBLE DIAMETER .8–.9 mm (α = .28 to .31).

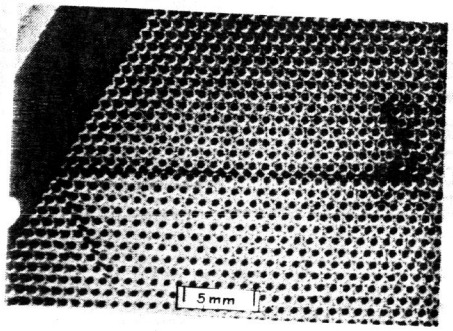

Fig. 13 STACKING FAULT SPREADING FROM A VACANCY ARRAY.

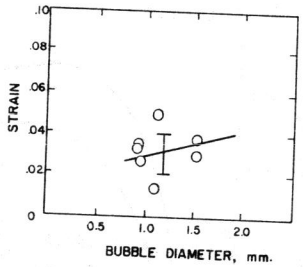

Fig. 15 STRAIN FOR GRAIN BOUNDARY FRACTURE

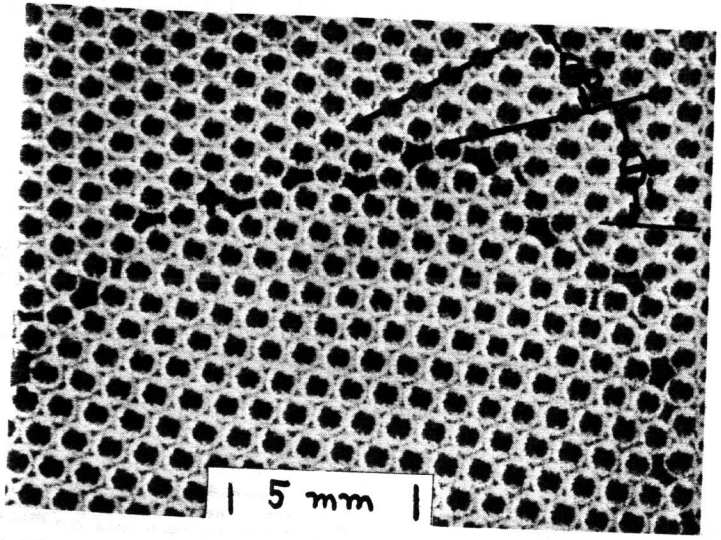

Fig. 14. GRAIN BOUNDARY. SHOWS INNER AND OUTER ANGLES